

Magnetic phase diagram of single-layer $CrBr_3$

Wei Jiang(江伟), Yue-Fei Hou(侯跃飞), Shujing Li(李淑静), Zhen-Guo Fu(付振国), and Ping Zhang(张平)
Citation: Chin. Phys. B, 2021, 30 (**12**): 127501. DOI: 10.1088/1674-1056/ac0043
Journal homepage: http://cpb.iphy.ac.cn; http://iopscience.iop.org/cpb

What follows is a list of articles you may be interested in

Spin orbit torques in Pt-based heterostructures with van der Waals interface

Qian Chen(陈倩), Weiming Lv(吕伟明), Shangkun Li(李尚坤), Wenxing Lv(吕文星), Jialin Cai(蔡佳林), Yonghui Zhu(朱永慧), Jiachen Wang(王佳晨), Rongxin Li(李荣鑫), Baoshun Zhang(张宝顺), and Zhongming Zeng(曾中明)
Chin. Phys. B, 2021, 30 (**9**): 097506. DOI: 10.1088/1674-1056/ac0908

Optimized growth of compensated ferrimagnetic insulator $Gd_3Fe_5O_{12}$ with a perpendicular magnetic anisotropy

Heng-An Zhou(周恒安), Li Cai(蔡立), Teng Xu(许腾), Yonggang Zhao(赵永刚), and Wanjun Jiang(江万军)
Chin. Phys. B, 2021, 30 (**9**): 097503. DOI: 10.1088/1674-1056/ac0db0

Magnetic dynamics of two-dimensional itinerant ferromagnet Fe_3GeTe_2

Lijun Ni(倪丽君), Zhendong Chen(陈振东), Wei Li(李威), Xianyang Lu(陆显扬), Yu Yan(严羽), Longlong Zhang(张龙龙), Chunjie Yan(晏春杰), Yang Chen(陈阳), Yaoyu Gu(顾耀玉), Yao Li(黎遥), Rong Zhang(张荣), Ya Zhai(翟亚), Ronghua Liu(刘荣华), Yi Yang(杨燚), and Yongbing Xu(徐永兵)
Chin. Phys. B, 2021, 30 (**9**): 097501. DOI: 10.1088/1674-1056/ac0e25

Magnetocrystalline anisotropy and dynamic spin reorientation of half-doped $Nd_{0.5}Pr_{0.5}FeO_3$ single crystal

Haotian Zhai(翟浩天), Tian Gao(高湉), Xu Zheng(郑旭), Jiali Li(李佳丽), Bin Chen(陈斌), Hongliang Dong(董洪亮), Zhiqiang Chen(陈志强), Gang Zhao(赵钢), Shixun Cao(曹世勋), Chuanbing Cai(蔡传兵), and Vyacheslav V. Marchenkov
Chin. Phys. B, 2021, 30 (**7**): 077502. DOI: 10.1088/1674-1056/ac0786

Experiments and SPICE simulations of double MgO-based perpendicular magnetic tunnel junction

Qiuyang Li(李求洋), Penghe Zhang(张蓬鹤), Haotian Li(李浩天), Lina Chen(陈丽娜), Kaiyuan Zhou(周恺元), Chunjie Yan(晏春杰), Liyuan Li(李丽媛), Yongbing Xu(徐永兵), Weixin Zhang(张卫欣), Bo Liu(刘波), Hao Meng(孟浩), Ronghua Liu(刘荣华), and Youwei Du(都有为)
Chin. Phys. B, 2021, 30 (**4**): 047504. DOI: 10.1088/1674-1056/abdea2

Magnetic phase diagram of single-layer $CrBr_3$*

Wei Jiang(江伟)[1], Yue-Fei Hou(侯跃飞)[1], Shujing Li(李淑静)[2], Zhen-Guo Fu(付振国)[1], and Ping Zhang(张平)[1,3,†]

[1] *Institute of Applied Physics and Computational Mathematics, Beijing* 100088, *China*
[2] *Beijing University of Chemical Technology, Beijing* 100029, *China*
[3] *School of Physics and Physical Engineering, Qufu Normal University, Qufu* 273165, *China*

(Received 22 March 2021; revised manuscript received 5 May 2021; accepted manuscript online 12 May 2021)

We theoretically provide a magnetic phase diagram for the single-layer (SL) $CrBr_3$, which could be effectively tuned by both strain engineering and charge doping in SL-$CrBr_3$. Through systematical first-principles calculations and Heisenberg model Hamiltonian simulations, three different magnetic phases in SL-$CrBr_3$, which are off-plane ferromagnetic, in-plane ferromagnetic and in-plane Néel-antiferromagnetic phases, are found in the strain and charge doping regimes we studied. Furthermore, our results show that higher order Heisenberg exchange parameters and anisotropy exchange parameters should be taken into account for accurately illustrating the magnetic phase transition in SL-$CrBr_3$. As a result, we find from the SpinW simulation that the Curie temperature is about $T_c = 38.4$ K, which is well consistent with the experimental result 34 K [*Nano Lett.* **19** 3138 (2019)]. The findings here may be confirmed in future experiments, and may be useful for the potential applications of SL-$CrBr_3$ in spintronics field.

Keywords: magnetic anisotropy, single-layer $CrBr_3$, Néel-antiferromagnetic phase

PACS: 75.30.Gw, 75.30.Kz, 75.50.Ee, 75.70.Ak **DOI:** 10.1088/1674-1056/ac0043

1. Introduction

Since the discovery of graphene,[1,2] the two-dimensional (2D) materials have attracted a lot of interests during the past two decades. 2D materials become very important in modern condensed matter physics and introduce many novel ideas to our communities. The electronic and optical properties have been studied explosively in graphene, silicene, and transition metal dichalcogenides,[3–5] etc., but the 2D magnet is still a part to be further studied. The reason may be, differing from the bulk materials, that the long-range magnetic order in 2D materials is prohibited[6–8] by Mermin–Wagner theorem at finite temperature.[9] However, more and more studies reveal that magnetic anisotropy, which originates mainly from spin-orbit coupling,[10] can overcome this restriction and thus becomes an important parameter for 2D magnets.

In recent years, many intrinsic ferromagnetisms in atomically thin magnets have been widely studied in various van der Waals materials, including rare-earth chalcohalides REChX (RE = rare earth; Ch = O, S, Se, Te; X = F, Cl, Br, I),[11] metallic Fe_3GeTe_2,[12–14] semiconducting $Cr_2Ge_2Te_6$[15,16] and insulating CrI_3.[17–19,23–29] Among them, single-layer $CrBr_3$ (SL-$CrBr_3$) gradually attracted the attention of scientists. For example, recently, Zhang *et al.* have experimentally demonstrated the intrinsic ferromagnetism in SL-$CrBr_3$ and reported the spontaneous magnetization persistence with a Curie temperature of 34 K.[30] The magnon-assisted tunneling and the magnetic proximity effects in van der Waals heterostructures based on $CrBr_3$ have also been widely studied.[31–34] For example, the charge-state dependency of the magnetic proximity effects in $MoSe_2/CrBr_3$ van der Waals heterostructures has been studied via low-temperature magneto-optical spectroscopy experiments, which conformed with that the valley polarization of the $MoSe_2$ trion state may be remarkably related to the local $CrBr_3$ magnetization, while the neutral exciton state remains insensitive to the ferromagnet.[32] These discoveries provide us sufficient opportunities for both fundamental studies and spintronics applications.

Compared with the vigorous development of experimental research, the theoretical research on the magnetism of SL-CrX_3 is somewhat lacking. In-depth understanding and control of the magnetic properties of SL-CrX_3 will help the development of low-dimensional spintronic devices based on SL-CrX_3. Strain engineering and charge doping are two widely used methods to introduce new phases and effectively tune magnetic properties of the 2D structures.[19–22,35–39] For instances, on one hand, in strain engineering, Lucas *et al.* have reported the strain-tunable magnetic anisotropy energy (MAE) in 2D SL-CrX_3 (with X = Cl, Br, and I),[36] and on the other hand, charge doping is applied to tune the magnetic properties of SL-CrI_3.[19]

To our knowledge, up to now, the influences of strain and charge doping on the magnetic properties of SL-$CrBr_3$ have not been discussed in detail in the present literatures. However, a detailed understanding on fundamental properties of SL-$CrBr_3$ plays an important role in realizing its potential ap-

*Project supported by the National Natural Science Foundation of China (Grant No. 11625415). Z.-G. Fu acknowledges the Innovation Development Foundation of China Academy of Engineering Physics (Grant No. ZYCX1921-02).

†Corresponding author. E-mail: zhang_ping@iapcm.ac.cn

© 2021 Chinese Physical Society and IOP Publishing Ltd

plications in spin-base technologies. Owing to the interest and importance from the perspectives of both basis physics and potential applications of SL-$CrBr_3$ in the fields of spintronics, it is timely to provide a theoretical analysis of the magnetic phases of SL-$CrBr_3$ tuned by strain effect and charge doping. Therefore, in this work, by employing systematical first-principals calculations and Heisenberg model simulations, we theoretically investigate the magnetic phase transitions in SL-$CrBr_3$ induced by reasonable strains and charge doping. Three different magnetic ground states, including off-plane ferromagnetic (FM), in-plane FM and in-plane Néel-antiferromagnetic (Néel-AFM) phases, are found in our calculations. Furthermore, a Heisenberg Hamiltonian, which takes into account the third-nearest-neighbor Heisenberg exchange parameter and next-nearest-neighbor anisotropy exchange parameter, is used to accurately explain the magnetic phase transition in SL-$CrBr_3$. The Curie temperature we obtained is about $T_C = 38.4$ K, which is in good agreement with the experimental result 34 K.[30]

2. Calculation details

Our density functional theory (DFT)[40,41] calculations are performed by using the Vienna *ab initio* simulation package.[42] The exchange–correlation functional is subjected to the generalized gradient approximation (GGA) in Perdew, Burke, and Ernzerhof (PBE) form.[43] Core electrons are treated with the projected augmented wave (PAW) method[44–46] and the valence electrons are calculated on a plane wave basis with a cut-off energy of 350 eV. The vacuum space is chosen as 15 Å, which is large enough to avoid the layered interactions. A $9\times9\times1$ Monkhorst k-point mesh is set for Brillouin zone integrations. All structures are optimized until the total energy is converged to be with 10^{-8} eV and the Hellmann–Feynman force on each atom is smaller than 0.001 eV/Å. To characterize the stability of SL-$CrBr_3$, we also calculate the elastic constant by employing AELAS code.[47] To extract both Heisenberg exchange parameters and anisotropy exchange parameters, a three-neighbor XXZ Heisenberg model Hamiltonian[19] is employed to fit the total energies in our DFT calculations for different spin configurations on a honeycomb lattice. In addition, the Curie temperature is estimated by using SpinW[48] simulations in which a $100\times100\times1$ honeycomb lattice is used. The SpinW simulations involve 10^4 Monte–Carlo (MC) steps per site in order to accurately obtain thermal equilibrium for each temperature. In the following text, the level of doped carriers per Cr atom is expressed as $\delta n = n - n_0$ (in units of e/Cr), where the intrinsic valence electron number of each Cr atom, and positive and negative values represent electron doped (e-doped) and hole doped (h-doped) states, respectively. For strained SL-$CrBr_3$, the quantity of strain is defined as $\varepsilon = (a - a_0)/a_0$, where a and a_0 are the horizontal lattice constants of the strained and the intrinsic SL-$CrBr_3$, respectively.

3. Results and discussion

The optimized atomic structure of SL-$CrBr_3$ is shown in Figs. 1(a) and 1(b). For the intrinsic structure, Cr atoms share a honeycomb lattice with a lattice constant $a_0 = 6.44$ Å. Six Br atoms constitute a slightly distorted octahedron around each Cr atom. Here, we consider four spin configurations to realize the FM, Néel-AFM, stripy-antiferromagnetic (stripy-AFM), zigzag-antiferromagnetic (zigzag-AFM) orders, as plotted in Figs. 1(c)–1(f). Both off-plane and in-plane orientations of magnetic moment of Cr are calculated to analyze the magnetic phase and MAE. In order to systematically study the magnetic states of SL-$CrBr_3$, the calculations on strain and charge effects are performed. In the following calculations, the strain strength ε changes from -10% to 15%, and the doped carriers δn changes from -0.25 to 0.25.

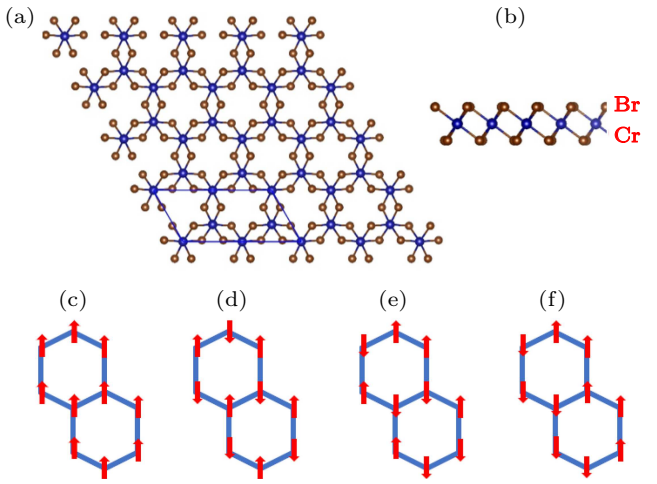


Fig. 1. Top (a) and side (b) views of SL-$CrBr_3$ atomic structure. The blue parallelogram in (a) shows the unit cell. FM, Neel-AFM, stripy-AFM and zigzag-AFM orders are shown in (c)–(f), respectively, where the red arrows represent the spin orientations.

Before discussing the magnetic orders of SL-$CrBr_3$, which are tuned by strain and charge doping, it is necessary to clarify whether the structure of SL-$CrBr_3$ is stable under external strain. Our DFT calculations show that the 2D Young's modulus of SL-$CrBr_3$ is 27 N/m, which is nearly an order smaller than that of graphene (340 N/m)[49] and SL-MoS_2 (180 N/m).[50] This means that SL-$CrBr_3$ is much softer comparing with other typical 2D magnets. Therefore, it is possible for us to explore the magnetic phase diagram of SL-$CrBr_3$ in a large range of strain and charge doping. In addition, the stability of SL-$CrBr_3$ under strain and charge modulations are also carefully checked by phonon dispersion calculations by using the phonopy code.[51] The phonon results, which are not shown for briefness, show that the structure of SL-$CrBr_3$ is stable in the strain and doping regimes we considered in this work. The stability of SL-$CrBr_3$ may make it a promising

candidate for the potential application in the low-dimensional spintronics.

Now let us discuss the magnetic phase modulations of SL-$CrBr_3$ in terms of strain and charge doping. We start from the effect of strain without charge doping (i.e., $\delta n = 0$). The total energy differences ΔE (in meV/Cr) of SL-$CrBr_3$ in different antimagnetic orders relative to the off-plane FM order as functions of strain strength ε are plotted in Fig. 2, where black squares, red dots, and blue triangles are for zigzag-AFM, stripy-AFM, and Néel-AFM, respectively. It is clear to us that if there is no external strain, all three types of AFM present higher ground state energy than that of FM order, which agrees with the experimental observation that SL-$CrBr_3$ is ferromagnetic at the intrinsic structure.[30] Furthermore, more detailed calculations for the intrinsic SL-$CrBr_3$ without strain and doping indicate that (i) the off-plane FM order has the lowest total energy (denoted by $E_{\rm tot}^{\rm off}$), and the MAE for FM orders is $E_{\rm MA} = E_{\rm tot}^{\rm in} - E_{\rm tot}^{\rm off} = 0.22$ meV/Cr with $E_{\rm tot}^{\rm in}$ being the total energy of in-plane FM order; and (ii) the metastable AFM phase is zigzag-AFM, whose total energy is about $\sim$16.22 meV/Cr, which is higher than that of off-plane FM (see the black squares in Fig. 2). Under the compressed strain ($\varepsilon<0$), the energy curves of SL-$CrBr_3$ move down and turn to be negative at $\varepsilon = -4.2\%$ as shown in Fig. 2, which corresponds to the magnetic phase transition from off-plane FM to Néel-AFM order. While if SL-$CrBr_3$ is stretched ($\varepsilon > 0$), the total energies of AFM orders are always positive as shown in Fig. 2, which indicates that off-plane FM order keeps unchanged when the stretching strain is loaded on.

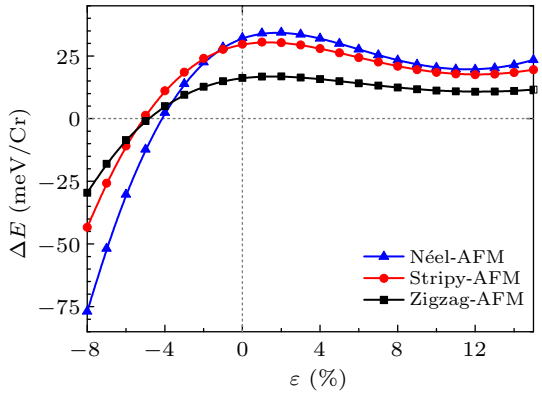


Fig. 2. Total energy differences ΔE (in meV/Cr) of SL-$CrBr_3$ in zigzag-AFM (black squares), stripy-AFM (red dots), and Néel-AFM (blue triangles) orders relative to the off-plane FM order as functions of strain strength ε.

Since the origin of long-range intrinsic ferromagnetism originates from magnetic anisotropy,[30] the modulation of strain effect on the MAE is also quantitatively analyzed in this work. The corresponding results are represented in Fig. 3. We can see that the magnetic anisotropies for each magnetic order are similar to each other. For SL-$CrBr_3$ with normal lattice constant, the magnitude of MAE is about $\sim$220 μeV/Cr, which is smaller than that in SL-CrI_3 (800 μeV/Cr).[19] This is possibly due to the stronger spin–orbital coupling (SOC) effect in I atom than that in Br atom. When SL-$CrBr_3$ is biaxially compressed (i.e., $\varepsilon < 0$), MAE turns smaller. In the Néel-AFM phase, MAE of SL-$CrBr_3$ is negative, which means that the spin orientation is in-plane, and thus the stable magnetic phase is in-plane Néel-AFM. If the stretching strain is applied, the MAE slowly increases at first and then gradually decreases with the increase of the strain intensity. When $\varepsilon = 9\%$, the MAE reaches the maximum value. Here, MAE is always positive, which indicates that the spin orientation for FM order is off-plane. Therefore, the stable magnetic phase should be off-plane FM when SL-$CrBr_3$ is stretched.

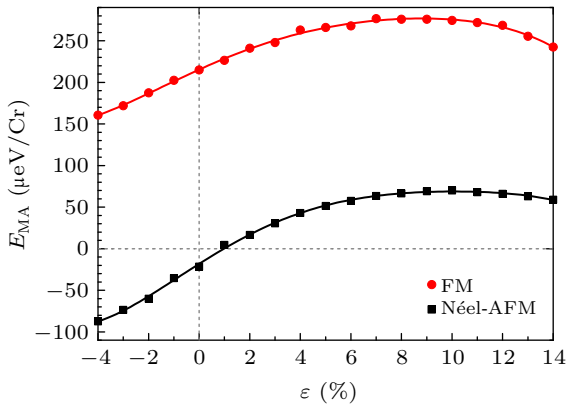


Fig. 3. Magnetic anisotropy energies $E_{\rm AM}$ (in units of μeV/Cr) for FM (red dots), and Néel-AFM (black squares) of SL-$CrBr_3$ as functions of strain strength ε.

To explore the physical mechanism of magnetic properties of SL-$CrBr_3$ under strain ($\varepsilon \neq 0$) without charge doping ($\delta n = 0$), a three-neighbor XXZ Heisenberg model Hamiltonian[19] is employed. Explicitly, the effective magnetic energy terms in different magnetic phases considered in this work are expressed as

$$H_{\rm FM} = 2(3J_1+6J_2+3J_3)\boldsymbol{S}_1\cdot\boldsymbol{S}_2+6(\lambda_1+2\lambda_2)S_1^zS_2^z+\delta, \quad (1)$$

$$H_{\rm Néel} = 2(-3J_1+6J_2-3J_3)\boldsymbol{S}_1\cdot\boldsymbol{S}_2-6(\lambda_1-2\lambda_2)S_1^zS_2^z+\delta, \quad (2)$$

$$H_{\rm Stripy} = 2(-J_1-2J_2+3J_3)\boldsymbol{S}_1\cdot\boldsymbol{S}_2-6(\lambda_1-2\lambda_2)S_1^zS_2^z+\delta, \quad (3)$$

$$H_{\rm Zigzag} = 2(J_1-2J_2-3J_3)\boldsymbol{S}_1\cdot\boldsymbol{S}_2-6(\lambda_1-2\lambda_2)S_1^zS_2^z+\delta, \quad (4)$$

where the first-, second-, and third-nearest-neighbor Heisenberg exchange parameters J_n ($n = 1,2,3$), as well as the first and second anisotropy exchange parameters λ_n ($n = 1,2$) are considered, $\boldsymbol{S}_{i=1,2}$ denote the spin of Cr. Here, J_2 and J_3 are needed to accurately analyze the magnetic phase and estimate the curie temperature in turn. λ_1 is good enough to explain the magnetic anisotropy at zero strain but it is necessary to take λ_2 into consideration under large compressive or tensile strain. In our calculations, the magnetic moment of Cr atoms is about 3.0 $\mu_{\rm B}$. Compared with the non-doped and unstrained cases, DFT calculations show that the magnetic moment of Cr atoms varies less than ±5% with the strain intensity and doping concentration. Therefore, in the fitting of the Heisenberg model

parameters, the dependence of the magnetic moment on strain and charge doping is ignored.

The fitted Heisenberg exchange parameters are shown in Fig. 4(a). It is obvious that J_1 has the largest magnitude and dominates the magnetic states in SL-$CrBr_3$. In briefness, J_1 is negative when system is in FM phase while positive when system is in AFM phase. This can be easily understood since J_1 represents the exchange interaction between the nearest-neighbor Cr atoms. With increasing the strain from -8% to 15%, the second-nearest and third-nearest neighboring effects become weaker so that J_2 and J_3 become smaller in magnitude, which could be obviously seen from Fig. 4(a). Since $CrBr_3$ honeycomb lattice presents two sub-lattices, J_2 acts within each sub-lattice and J_3 acts between the two sub-lattices. In SL-$CrBr_3$, J_2 is always negative and J_3 is always positive. The negative sign of J_2 indicates that the atoms within one sub-lattices favor to align ferromagnetically, while the positive sign of J_3 indicates that two sub-lattice favor to align antiferromagnetically.

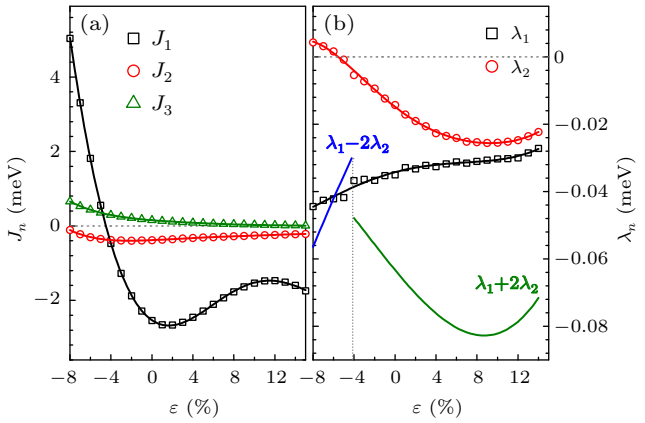


Fig. 4. (a) Fitted Heisenberg exchange parameters J_n $(n=1,2,3)$, and (b) anisotropy exchange parameters λ_n $(n=1,2)$ as functions of strain strength ε in SL-$CrBr_3$ without charge doping ($\delta n=0$). The curves of $\lambda_1-2\lambda_2$ (blue curve) and $\lambda_1+2\lambda_2$ (green curve) are also plotted in (b).

The fitted anisotropy exchange parameters are shown in Fig. 4(b). λ_1 is always negative and has larger magnitude. λ_2 is negative when $\varepsilon > -6\%$ and becomes positive when SL-$CrBr_3$ is heavily compressed. We know from Fig. 1(a) that each Cr atom has three nearest Cr atoms and six second-neighbor Cr atoms, and thus the MAE should be proportional to $\lambda_1+2\lambda_2$ ($\lambda_1-2\lambda_2$) for FM (AFM) order. It is clearly shown by the green cure in Fig. 4(b) that when $\varepsilon > -4.2\%$, $\lambda_1+2\lambda_2$ is always negative, and thereby the orientation for FM order is always off-plane in our strain range. Similarly, $\lambda_1-2\lambda_2$ is negative when $\varepsilon < -4.2\%$, which indicates that the orientation for Néel-AFM phase is in-plane (see the blue curve in Fig. 4(b)).

Based on our calculations, J_n $(n=1,2,3)$ are much larger than λ_n $(n=1,2)$, and J_1 is the largest in magnitude. As depicted in Fig. 2, the relative stable AFM phase at the intrinsic structure is zigzag-AFM. We adopt the Hamiltonian of FM and zigzag-AFM order to estimate Curie temperature for the intrinsic SL-$CrBr_3$ with a lattice constant a_0. The result of our SpinW simulations is $T_C = 38.4$ K, which is well consistent with the experimental result 34 K.[30] We also perform calculations only considering the nearest neighbor Heisenberg exchange parameter J_1 and first anisotropy exchange parameter λ_1. The corresponding Curie temperature is estimated as $T_C = 40.1$ K, which becomes worse comparing with the experimental result. Therefore, we believe that our three-neighbor XXZ Heisenberg model Hamiltonian is more accurate since it can contain more magnetic orders.

All above analysis are for the strain effect on the magnetic order transitions in SL-$CrBr_3$. In the absence of charge doping, external strain induces a magnetic phase transition between off-plane FM order and in-plane Néel-AFM order in SL-$CrBr_3$, which is different from the case of SL-CrI_3.[19] Following the same way, one could investigate the effect of charge doping with and/or without strain on the magnetic order transitions in SL-$CrBr_3$. Here, for briefness, we will not discuss the case that only charge doping effect is taken into account. Therefore, we explore the magnetic phase diagram via strain engineering and charge doping. The result is shown in Fig. 5. From Fig. 5, we can clearly see that in the strain and charge doping regimes we studied, there are three different magnetic phases in SL-$CrBr_3$, which are off-plane FM (green region), in-plane FM (yellow region) and in-plane Néel-AFM (cyan region). There are at least four points need to be noticed in Fig. 5: (i) Consistent with the aboe discussions, for the intrinsic SL-$CrBr_3$ ($\varepsilon = 0$ and $\delta n = 0$), the magnetic ground state should be off-plane FM order. (ii) If there is no charge doping ($\delta n = 0$) in the system but with certain strain (i.e., ε changes from -10% to 15%), SL-$CrBr_3$ will undergo a magnetic phase transition from the in-plane Néel-AFM to the off-plane FM. The corresponding phase transition point is about $\varepsilon = -4.2\%$, which is also in agreement with above analysis. (iii) Conversely, if strain is not applied on the system ($\varepsilon = 0$) but there exists charge doping ($\delta n \neq 0$), Fig. 5 shows that as the doping concentration increases from negative value to positive value, the magnetic ground state will be modulated from the off-plane FM into the in-plane FM. The phase transition point is at the doping concentration of $\delta n = 0.06$ e/Cr (see point A marked in Fig. 5), (iv) The magnetic phase of the system could be simultaneously modulated by charge doping and external strain. Through detailed calculations, the phase boundaries among three different magnetic phases are obtained (see the black curves in Fig. 5). The intersection of the three magnetic phases is approximately at $\varepsilon = -4.2\%$ and $\delta n = 0.07$ e/Cr (see point B marked in Fig. 5). In detail, the phase boundary between in-plane Néel-AFM and in-plane FM is localized at $\varepsilon = -4.2\%$. In other words, when $\delta n > 0.07$ e/Cr, the phase transition between in-plane Néel-AFM and in-plane FM responds significantly to the strain effect. In this case, when the

strain is slightly greater (less) than −4.2%, the system will come into in-plane FM (Néel-AFM) order. When the charge doping is less than 0.07 *e*/Cr, with the compressive biaxial strain increasing, the system tends to transform from off-plane FM to in-plane Néel-AFM.

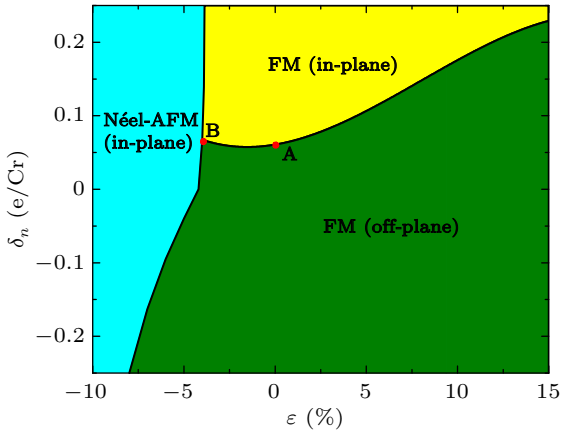


Fig. 5. Magnetic phase diagram of SL-$CrBr_3$ in the strain and charge doping regimes. Point A represents the phase transition at intrinsic structure with a normal lattice constant a_0. Point B indicates the intersection of three magnetic phases.

4. Conclusion

In summary, we applied DFT calculations and model Hamiltonian simulations to investigate the magnetic properties of the recently discovered 2D ferromagnet, SL-$CrBr_3$. The ground state is confirmed to be FM, which is consistent with the previous experiment. $CrBr_3$ exhibits strong magnetic anisotropy (215 μeV/Cr) with an off-plane easy axis. We studied the effect of strain engineering and charge doping on SL-$CrBr_3$, and provided a magnetic phase diagram with rich tunable physics. The magnetic properties are remarkably dominated by strain, which have extensive impact on local spin and thus dominate the phase transition between the FM and AFM phases. Under particular strain, charge doping (especially hole doping) can also modulate the spin orientation and in turn manipulate magnetic states. Based on our fitted Heisenberg exchange parameters and anisotropy exchange parameters, we systematically analyzed the magnetic properties and estimated Curie temperature as 38.4 K. We also found that phase transition from the FM order to the Néel-AFM order is dominated by the nearest-neighbor exchange parameter J_1, while the phase transition from the off-plane FM to the in-plane FM is influenced by MAE. The rich tunable magnetic properties make SL-$CrBr_3$ a reliable and promising candidate for potential application in spintronics.

References

[1] Novoselov K S, Geim A K, Morozov S V, Jiang D, Zhang Y, Dubonos S V, Grigorieva I V and Firsov A A 2004 *Science* **306** 666

[2] Castro Neto A H, Guinea F, Peres N M R, Novoselov K S and Geim A K 2009 *Rev. Mod. Phys.* **81** 109

[3] Bonaccorso F, Colombo L, Yu G, Stoller M, Tozzini V, Ferrari A C, Ruoff R S and Pellegrini V 2015 *Science* **347** 1246501

[4] Zhong F, Wang H, Wang Z, Wang Y, He T, Wu P, Peng M, Wang H, Xu T, Wang F, Wang P, Miao J and Hu W 2020 *Nano Res.* **14** 1840

[5] Li Y, Zhou Z, Zhang S and Chen Z 2008 *J. Am. Chem. Soc.* **130** 16739

[6] McGuire M A, Dixit H, Cooper V R and Sales B C 2015 *Chem. Mater.* **27** 612

[7] Li X and Yang J 2014 *J. Mater. Chem. C* **2** 7071

[8] Zhang W B, Qu Q, Zhu P and Lam C H 2015 *J. Mater. Chem. C* **3** 12457

[9] Mermin N D and Wagner H 1966 *Phys. Rev. Lett.* **17** 1133

[10] Lado J L and Fernández-Rossier J 2017 *2D Mater.* **4** 035002

[11] Ji J, Sun M, Cai Y, Wang Y, Sun Y, Ren W, Zhang Z, Jin F and Zhang Q 2021 *Chin. Phys. Lett.* **38** 047502

[12] Deng Y, Yu Y, Song Y, Zhang J, Wang N Z, Sun Z, Yi Y, Wu Y Z, Wu S, Zhu J, Wang J,Chen X H and Zhang Y 2018 *Nature* **563** 94

[13] Fei Z, Huang B, Malinowski P, Wang W, Song T, Sanchez J, Yao W, Xiao D, Zhu X, May A F, Wu W, Cobden D H, Chu J H and Xu X 2018 *Nat. Mater.* **17** 778

[14] Chen X, Lin Z Z and Cheng L R 2021 *Chin. Phys. B* **30** 047502

[15] Gong C, Li L, Li Z, Ji H, Stern A, Xia Y, Cao T, Bao W, Wang C, Wang Y, Qiu Z Q, Cava R J, Louie S G, Xia J and Zhang X 2017 *Nature* **546** 265

[16] Tang X, Fan D, Guo L, Tan H, Wang S, Lu X, Cao X, Wang G and Zhou X 2018 *Appl. Phys. Lett.* **113** 263902

[17] Wang H, Fan F, Zhu S and Wu H 2016 *Europhys. Lett.* **114** 47001

[18] Huang B, Clark G, Navarro-Moratalla E, Klein D R, Cheng R, Seyler K L, Zhong D, Schmidgall E, McGuire M A, Cobden D H, Yao W, Xiao D, Jarillo-Herrero P and Xu X 2017 *Nature* **546** 270

[19] Zheng F, Zhao J, Liu Z, Li M, Zhou M, Zhang S B and Zhang P 2018 *Nanoscale* **10** 14298

[20] Wei W G, Wang H, Zhang K, Liu H, Kou Y F, Chen J J, Du K, Zhu Y Y, Hou D L, Wu R Q, Yin L F and Shen J 2015 *Chin. Phys. Lett.* **32** 87504

[21] Bai Y H, Wang X, Mu L P and Xu X H 2016 *Chin. Phys. Lett.* **33** 87501

[22] Zhao X, Hu Z, Yang Q, Peng B, Zhou Z and Liu M 2018 *Chin. Phys. B* **27** 097505

[23] Lin G T, Luo X, Chen F C, Yan J, Gao J J, Sun Y, Tong W, Tong P, Lu W J, Sheng Z G, Song W H, Zhu X B and Sun Y P 2018 *Appl. Phys. Lett.* **112** 072405

[24] Chen L, Chung J H, Chen T, Duan C, Schneidewind A, Radelytskyi I, Voneshen D J, Ewings R A, Stone M B, Kolesnikov A I, Winn B, Chi S, Mole R A, Yu D H, Gao B and Dai P 2020 *Phys. Rev. B* **101** 134418

[25] Lee I, Utermohlen F G, Weber D, Hwang K, Zhang C, van Tol J, Goldberger J E, Trivedi N and Hammel P C 2020 *Phys. Rev. Lett.* **124** 017201

[26] Soriano D, Katsnelson M I and Fernández-Rossier J 2020 *Nano Lett.* **20** 6225

[27] Choi Y, Ryan P J, Haskel D, McChesney J L, Fabbris G, McGuire M A and Kim J W 2020 *Appl. Phys. Lett.* **117** 022411

[28] Vanherck J, Bacaksiz C, Sorée B, Milošević M V and Magnus W 2020 *Appl. Phys. Lett.* **117** 052401

[29] Tiwari S, Van de Put M L, Sorée B and Vandenberghe W G 2021 *Phys. Rev. B* **103** 014432

[30] Zhang Z, Shang J, Jiang C, Rasmita A, Gao W and Yu T 2019 *Nano Lett.* **19** 3138

[31] Ghazaryan D, Greenaway M T, Wang Z, Guarochico-Moreira V H, Vera-Marun I J, Yin J, Liao Y, Morozov S V, Kristanovski O, Lichtenstein A I, Katsnelson M I, Withers F, Mishchenko A, Eaves L, Geim A K, Novoselov K S and Misra A 2018 *Nat. Electron.* **1** 344

[32] Lyons T P, Gillard D, Molina-Sánchez A, Misra A, Withers F, Keatley P S, Kozikov A, Taniguchi T, Watanabe K, Novoselov K S, Fernández-Rossier J and Tartakovskii A I 2020 *Nat. Commun.* **11** 6021

[33] Ciorciaro L, Kroner M, Watanabe K, Taniguchi T and Imamoglu A 2020 *Phys. Rev. Lett.* **124** 197401

[34] Huang B, McGuire M A, May A F, Xia D, Jarillo-Herrero P and Xu X 2020 *Nat. Mater.* **19** 1276

[35] Peng R, Xu H C, Tan S Y, Cao H Y, Xia M, Shen X P, Huang Z C, Wen C H P, Song Q, Zhang T, Xie B P, Gong X G and Feng D L 2014 *Nat. Commun.* **5** 5044

[36] Lucas W and Yan J A 2018 *Phys. Rev. B* **98** 144411

[37] Zhuang H L, Kent P R C and Hennig R G 2016 *Phys. Rev. B* **93** 134407

[38] Rajapitamahuni A, Zhang L, Koten M A, Singh V R, Burton J D, Tsymbal E Y, Shield J E and Hong X 2016 *Phys. Rev. Lett.* **116** 187201

[39] Lee J E, Ahn G, Shim J, Lee Y S and Ryu S 2012 *Nat. Commun.* **3** 1024

[40] Hohenberg P and Kohn W 1964 *Phys. Rev.* **136** B864
[41] Kohn W and Sham L J 1965 *Phys. Rev.* **140** A1133
[42] Kresse G and Furthmüller J 1996 *Phys. Rev. B* **54** 11169
[43] Perdew J P, Burke K and Ernzerhof M 1996 *Phys. Rev. Lett.* **77** 3865
[44] Blöchl P E 1994 *Phys. Rev. B* **50** 17953
[45] Kresse G and Joubert D 1999 *Phys. Rev. B* **59** 1758
[46] Blöchl P E, Först C J and Schimpl J B 2003 *J. B. Mater. Sci.* **26** 33
[47] Zhang S H and Zhang R F 2017 *Comput. Phys. Commun.* **220** 403
[48] Toth S and Lake B 2015 *J. Phys.: Condens. Matter* **27** 166002
[49] Kim K S, Zhao Y, Jang H, Lee S Y, Kim J M, Kim K S, Ahn J H, Kim P, Choi J Y and Hong B H 2009 *Nature* **457** 706
[50] Bertolazzi S, Brivio J and Kis A 2011 *ACS Nano* **5** 9703
[51] Togo A and Tanaka I 2015 *Scr. Mater.* **108** 1